https://doi.org/10.15407/ujpe71.5.478

SALAM KHALAF OMAR,[1] E.E. KHADEER [2]

[1] University Presidency, University of Telafer
(e-mail: Salamomar.sk@gmail.com)
[2] College of Science, University of Mosul
(e-mail: dr.adrees@uomosul.edu.iq)

STUDYING THE EFFECT OF THE WEIGHT FRACTIONS OF DIFFERENT TYPES OF POWDERS ON THERMAL CONDUCTIVITY AND HOMOGENEITY OF AN EPOXY BLEND RESIN

In this study investigated the effects of weight fractions (10–50 wt%) of carbon nanoparticles (CNP), Al_2O_3, NiO, and ZnO powders on the thermal conductivity and homogeneity of a 50 : 50 epoxy blend resin. Scanning electron microscopy (SEM) revealed distinct surface morphologies: NiO composites showed smooth surfaces with minimal gaps at low concentrations but developed large voids at 50 wt%, while Al_2O_3 surfaces exhibited fractures and increased blistering at higher loadings. ZnO and CNP composites displayed rough, porous surfaces with significant agglomeration at 50 wt%. Thermally, all fillers enhanced conductivity relative to the unreinforced epoxy (0.938 W/(m · K)), with NiO exhibiting the highest improvement (32.5–46.3%), followed by ZnO (28–38.7%), Al_2O_3 (19.5–31.3%), and CNP (11.2–16.7%). Homogeneity testing via γ-ray attenuation (^{241}Am source) demonstrated that ZnO composites achieved the highest homogeneity (lowest $\Delta\mu$% and standard deviation σ_μ = 0.004–0.02%), whereas NiO composites were the least homogeneous. Crucially, ZnO's uniform particle distribution also provided superior gamma-ray shielding (μ = 0.108–0.205 cm^{-1}), while NiO's heterogeneity compromised its attenuation efficacy.

Keywords: aluminum oxide (Al_2O_3), carbon nanoparticles (CNP), epoxy blend resin, gamma-ray attenuation, homogeneity test, nickel oxide (NiO), polymer composite, scanning electron microscopy (SEM), thermal conductivity, zinc oxide (ZnO).

1. Introduction

Epoxy resins, the most widely used thermoset materials in polymer composites, are typically synthesized by reacting epichlorohydrin with bisphenol. They exhibit strong bonding strength to diverse substrates, excellent chemical and environmental resistance, notable insulating properties, outstanding adhesion, toughness, high electrical resistance, durability across high and low temperatures, flexibility, and ease of bubble-free pouring or casting [1, 2]. Polymer blending is a common technique used to obtain properties absent in the original polymers; for instance, incorporating an elastomer into a stiff polymer can enhance ductility and impact resistance [3]. Particulate fillers modify the physical and mechanical properties of polymers in various ways. Their primary commercial

Citation: Omar Salam Khalaf, Khadeer E.E. Studying the effect of the weight fractions of different types of powders on thermal conductivity and homogeneity of an epoxy blend resin. *Ukr. J. Phys.* **71**, No. 5, 478 (2026). https://doi.org/10.15407/ujpe71.5.478.

objectives are cost reduction and increased stiffness [4, 5]. These materials, including diverse polymers and particle-reinforced polymer-matrix composites– find wide application in areas such as the electrical industry, military and commercial aircraft, heaters, electrodes, flooring, and high-temperature thermally durable composites [6, 7]. While polymers are frequently employed as insulating materials, significant research focuses on enhancing their properties, particularly thermal conductivity. High thermal conductivity is essential for efficient heat dissipation, maintaining lower operating temperatures and preventing dielectric failures caused by overheating [8]. Polymers inherently exhibit low thermal conductivity due to their relatively low atomic density, weak chemical bonds, complex crystal structures, and significant anharmonicity in molecular vibrations [9]. The constitutive properties of composite materials (e.g., electrical, mechanical, and thermal) are significantly influenced by the distribution of particles within the matrix. This distribution depends on the additive phase's concentration, particle size, inter-particle distance, and morphology [10, 11]. Common techniques for assessing homogeneity or distribution rely on attenuation characteristics, such as intensity differences and variations in the linear attenuation coefficient. These characteristics are further evaluated using mathematical equations incorporating statistical measures of distribution and variability, such as the standard deviation. Such analyses quantify the homogeneity index (or degree of homogeneity) of multiphase materials, often correlating with the local concentration of the additive and the concentration ratio [12].

2. Materials and Methods

2.1. Materials

This study utilized two types of polymeric substrates based on epoxy resin. The first was a Turkish-manufactured epoxy resin (22240 Innopure Floor Epoxy), characterized as a light liquid with a dark yellow tint, low density, and low viscosity. It employs a hardener-to-resin ratio of 3 : 2 at a specified temperature and has a density of (1.00 ± 0.05) kg/L at 20 °C. This resin was blended with a second epoxy resin, Casting Resin LS800, manufactured by Shenzhen BKC Testing (China). (LS800) exhibits good flow properties, natural defoaming, anti-yellowing properties, high transparency, a ripple-free surface, and can be cured at both room and elevated temperatures. Both epoxy systems utilize the same Turkish-manufactured hardener (22240 Innopure Floor Epoxy). The resin mixture solidifies upon hardener addition. The support materials (fines) incorporated were:

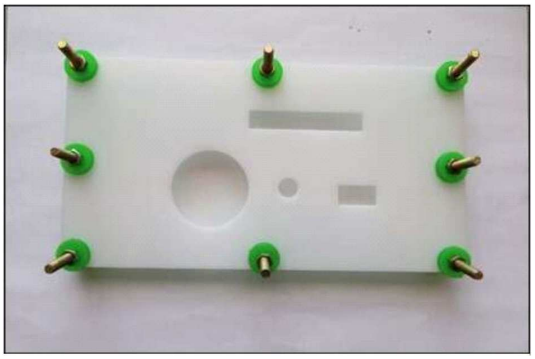

Fig. 1. Sample preparation mold

Nickel oxide (NiO): The primary oxide of nickel, classified as a basic metal oxide [13]. Supplied by Hopkin and Williams LTD (UK) with a particle size of (33 μm).

Carbon nanoparticles (CNP): Carbon-based materials with particle sizes on the nanoscale (supplied size: 89.77 nm). These particles attract scientific interest due to their distinctive architectures and unique chemical and physical properties [14]. Supplied by CNP (Any color, China).

Zinc oxide (ZnO): An inorganic compound widely used as a filler in materials and products including cosmetics, dietary supplements, rubber, plastics, ceramics, glass, and cement. While naturally occurring as zincite, the ZnO used was synthetic [15]. Supplied by Hopkin and Williams LTD (UK) with a particle size of (42 μm).

Aluminum oxide (Al_2O_3): The most prevalent form of aluminum oxide, used in composite fabrication. Also known as aloxide, aloxite, or alundum depending on specific forms or applications [16]. Supplied by BDH LTD (UK) with a particle size of 31 μm.

2.2. Sample preparation

The samples were fabricated using the hand-lay-up molding technique. This technique offers significant advantages, particularly the ability to produce large-volume, complex-shaped samples to desired dimensions without inherent size limitations, as demonstrated in Fig. 1. This contrasts with alternative pro-

Table 1. **The sample schematic diagram**

Mold type	Mold dimensions (mm)	International standards	Sample schematic diagram	Image of prepared samples
Thermal conductivity	5 × 41.16	Dimensions suitable for the analytical method	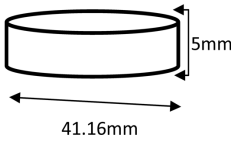	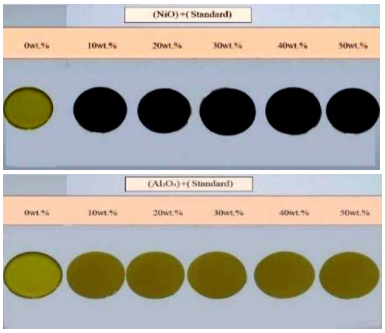
Homogeneity	5 × 14 × 90	Dimensions suitable for the analytical method	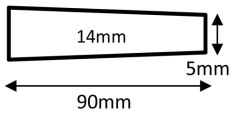	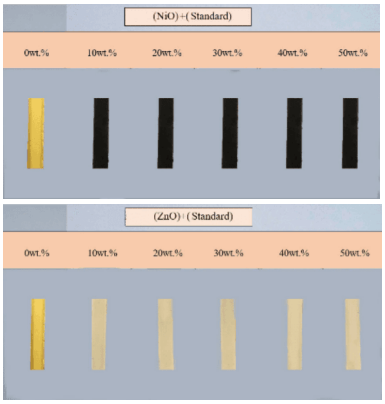

cesses, which are often more complex and may be size-constrained.

After oven drying, all fillers were sieved to the target granule size. The required quantities of filler were then measured using an electric balance with an accuracy of (0.001 gm). Composite samples were prepared by blending five different weight percentages (10, 20, 30, 40, and 50 wt%) of filler into the epoxy resin. The weight percentage was calculated as [17, 18]:

$$Wt\% = \frac{w_P}{w_c} \times 100\% = \frac{w_P}{w_P + w_m} \times 100\%. \quad (1)$$

The epoxy resin blend was weighed using an sensitive electrical balance to ensure the correct mixing ratio (4–10 g total). The filler powder was added to the epoxy resin and gently mixed for 15 min using a mechanical mixer in a clean container to achieve uniform particle dispersion. The hardener was then added gradually to the mixture under continuous stirring to minimize the formation of air bubbles. The resulting homogeneous mixture was poured into circular plastic molds (10 mm in diameter and × 2 mm in thickness). Samples were first left at room temperature for 24 hours to initiate hardening, then placed in an oven at 60 °C for 1 hour to complete polymerization. Finally, the entire assembly was allowed to cure at room temperature for 10 days.

2.3. Physical property tests

A physical property is any measurable characteristic that quantifies the state of a physical system [19]. Changes in a system's physical properties describe transitions between its transient states. These measurable characteristics are often termed observables. Crucially, physical properties are quantifiable; a measurable physical property is called a physical quantity. Based on the data and samples presented in Table 1, this study focuses on analyzing

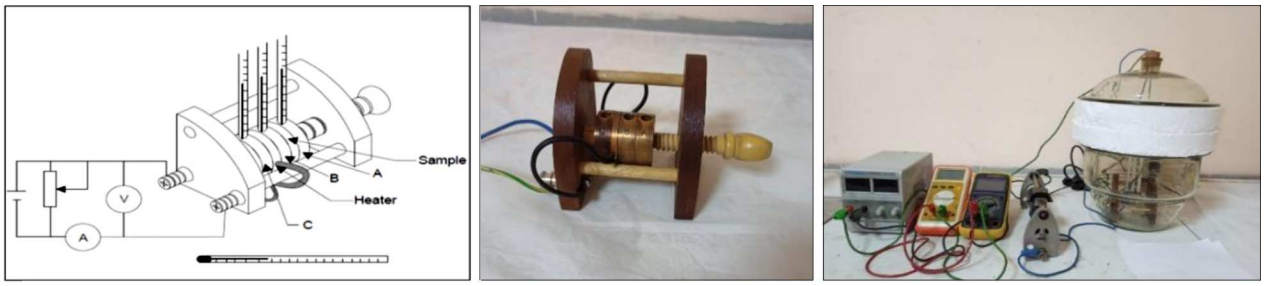

Fig. 2. Thermal conductivity testing device

the physical properties of Thermal Conductivity and Homogeneity.

2.4. Scanning electron microscope test

Scanning Electron Microscopy (SEM) is a high-resolution surface imaging and analytical technique that produces detailed nanoscale images of a sample's topography, enabling the detection of minute features such as cracks, voids, and particle distribution. It facilitates semi-quantitative chemical composition analysis at specific points and is widely applied to material failure investigation, quality control, and surface morphology studies across materials science, biology, and electronics. For this research, analyses were performed using an FEI Nova NanoSEM 450 at the University of Basrah. To ensure SEM imaging accuracy, all samples were sputter-coated with a thin gold layer (≈20 nm thickness) using a pulsed deposition system under high vacuum (10^{-5} bar). This minimized electrostatic charging and improved image resolution. The vacuum pressure in the FEI Nova NanoSEM 450 was maintained at 10^{-6} Torr to prevent electron scattering. Three random regions per sample were analyzed to ensure representative microstructural characterization.

2.5. Thermal conductivity test

The thermal conductivity of the samples was determined using a Lee's disc apparatus (manufactured by Griffin and George, UK), located in the Department of Physics, College of Science, University of Mosul (see Fig. 2).

The device operates on the principle of steady-state heat transfer from a heater through the sample to a cooled disc. It comprises three copper discs (A, B, and C), each 4.11 mm in diameter. Each disc features a radial hole drilled from the edge to accommodate a thermometer. A fourth disc, housing a 2.25-watt electric heating coil, shares the same diameter. For testing, a disc-shaped composite sample (with dimensions standardized according to Table 1) is placed between discs A and B. The heating coil is positioned between discs B and C and connected to a DC power supply. The voltage was fixed at 6 V and the current at 0.48 A. The entire assembly is thermally insulated to stabilize the ambient temperature. Upon energizing the heater, heat flows sequentially through the discs. Once thermal equilibrium is reached, the temperatures (T_A, T_B, T_C) recorded by the thermometers in each disc, along with the current and voltage, are noted. The thermal conductivity is then calculated from the heat flux (e) passing through the sample per unit area per second (W/m · K), using

$$e = \frac{V \cdot I}{[a_A T_A + a_S \frac{(T_A+T_B)}{2} + a_B T_B + a_C T_C]} \qquad (2)$$

and the (K) is calculated from

$$K = \frac{e \cdot d_s}{2\pi r^2 (T_B - T_A)} \left[a_s \frac{(T_A + T_B)}{2} + 2 a_A T_A \right]. \qquad (3)$$

Thermal conductivity measurements were repeated three times per sample to ensure statistical reliability. Temperature readings from mercury thermometers had a margin of error of ±0.1 °C, resulting in a maximum propagated error of ±3% in the thermal conductivity calculations (using error propagation formulas for Eqs (2) and (3)).

2.6. Homogeneity test

Homogeneity was tested using a Canberra amplifier device to calculate the absorption coefficient of a specific substance for gamma rays at multiple points within the sample. This testing was performed in the

a *b* *c*

Fig. 3. The equipment used in the homogeneity test: absorption coefficient measurement device (*a*); γ-source and lead layer (*b*); detector (*c*)

Physics Laboratories, Faculty of Science, University of Mosul, as shown in Fig. 3, *a*.

The sample intended for measuring the absorption coefficient was placed behind a lead shield. Measurements were conducted using a parallel gamma-ray beam from a ^{241}Am source, as shown in Fig. 3, *b*, with the power supply set to 850 V. The incident and transmitted gamma-ray intensities of the composite samples were measured using the detector shown in Fig. 3, *c*. Each measurement used a 30 s counting time. First, the incident radiation intensity (I_0) was measured, followed by the transmitted radiation intensity (I) through the sample. The percentage homogeneity ($\Delta\mu\%$) of the material was then calculated using [20]:

$$\Delta\mu\,(\%) = \frac{\mu' - \mu}{\mu'} \times 100\%. \tag{4}$$

Homogeneity was also assessed by calculating the standard deviation (σ_μ) of the linear attenuation coefficient over N measurements, derived from Eq. (5) [21]:

$$\sigma_\mu = \sqrt{\frac{\sum_{i=1}^{N} (\bar{\mu} - \mu_i)^2}{N-1}}, \tag{5}$$

where μ is the linear attenuation coefficient at a specific measurement point, $\bar{\mu}$ is the mean linear attenuation coefficient, and N is the number of measurement points on the sample.

3. Result And Discussion

3.1. Structural properties results

It is well-established that the filler-matrix interaction critically influences composite properties. To assess this interaction, the microstructure of both unreinforced and reinforced composites was characterized using scanning electron microscopy (SEM). SEM was selected for its superior analytical capabilities, offering magnifications up to 2 million times and high resolution (typically down to the nanometer scale), far exceeding that of optical microscopy. This enabled precise characterization of filler particle morphology and distribution within the polymer blend matrix. Fig. 6 shows representative SEM images of the unreinforced matrix at various magnifications.

The analysis of the images reveals a semi-homogeneous surface structure characterized by sparse grains and voids. At higher magnification (Fig. 4, *b*), the surface exhibits significant roughness, consisting of aggregated plate-like structures. Confined gaps are formed between these plates, potentially resulting from interactions between different epoxy resins. The presence of airborne dust particles, likely introduced during sample preparation, or base material grains dislodged during prior sample polishing, may also contribute to this morphology. Fig. 5 shows the surface morphology of the filler-reinforced polymer blend composite at a magnification of 25,000.

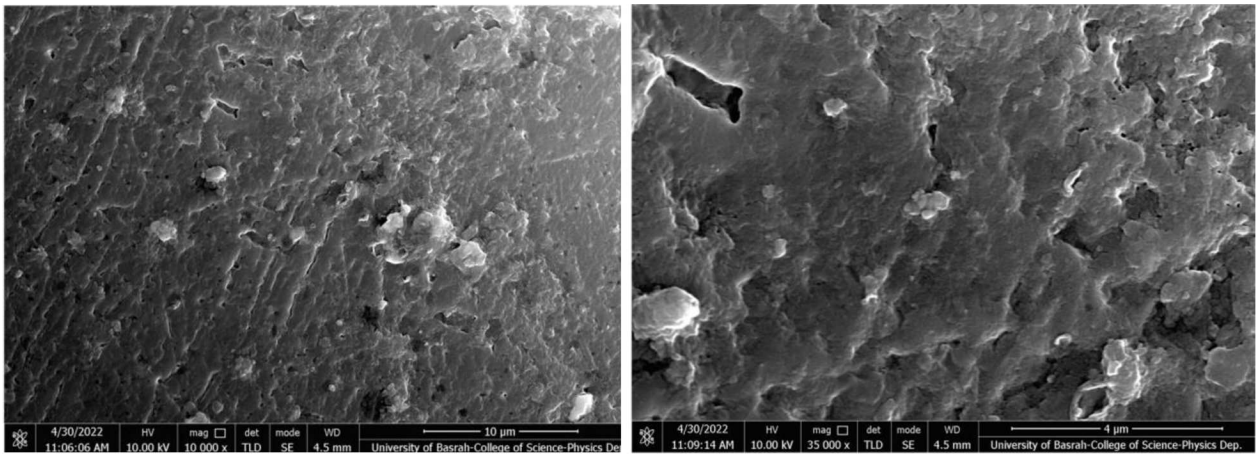

a *b*

Fig. 4. SEM images of the 0wt.% sample at different magnifications: 10000X (*a*); 35000X (*b*)

Samples reinforced with 10 wt.% NiO powder exhibited smooth surfaces with minimal cavity formation. However, localized blistering was observed on the surface, likely attributable to the rupture of air bubbles during sample preparation [22]. At higher reinforcement concentrations (50 wt.%), the surface became smoother overall but developed large voids in specific regions. These voids resulted from the coalescence of smaller cavities, potentially caused by manufacturing artifacts or increased particle agglomeration at elevated powder loading. For composites reinforced with other powder types, particularly the sample containing 10 wt.% Al_2O_3 powder (Fig. 5, *c*), the surface appears smooth but contains numerous cracks and voids, along with minor blisters. However, as the filler powder concentration increases to 50 wt.%, these blisters rapidly increase in size, developing into agglomerations arranged in the form of sheets or flakes. Concurrently, the surface becomes significantly rougher, undulating, and porous due to a substantial increase in voids. This deterioration results from enhanced particle accumulation as the powder concentration rises, causing the powder to separate from the resin as aggregates during sample preparation. Furthermore, the high viscosity induced by the increased powder loading impedes the complete growth of the polymeric chains, leading to premature solidification. This reduces the time available for uniform powder distribution throughout the composite sample [23]. The surfaces of composites filled with 10 wt.% ZnO or CNP powder (Figs 5, *b* and 5, *d*) appeared rough, undulating, and blistered, indicating brittleness. Microscopy also revealed micro-cracks, agglomerations, and particle clustering. Increasing the reinforcing powder concentration to 50 wt.% altered the surface morphology significantly. The ZnO-filled composite exhibited a smoother surface, largely free of microdefects like cracks and voids, though scattered blisters remained. In contrast, the CNP-filled composite developed a greater number of larger voids compared with its lower-concentration counterpart. This difference arises from increased particle agglomeration at higher powder concentrations, causing the powder to separate from the resin as lumps during preparation. Additionally, the high viscosity induced by these powder loadings impeded complete polymeric chain growth. This led to premature solidification, depriving the powder of sufficient time to distribute uniformly throughout the composite sample [24].

3.2. Physical property results

3.2.1. Thermal conductivity results

The thermal conductivity of the epoxy blend resin was measured both before and after reinforcement with the filler powders. This property is crucial for evaluating how changes in the resin's composition affect the material behavior under thermal gradients. For the prepared samples, thermal conductivity values were calculated using temperatures obtained from a Lee's disk apparatus and applying Eqs. (2)

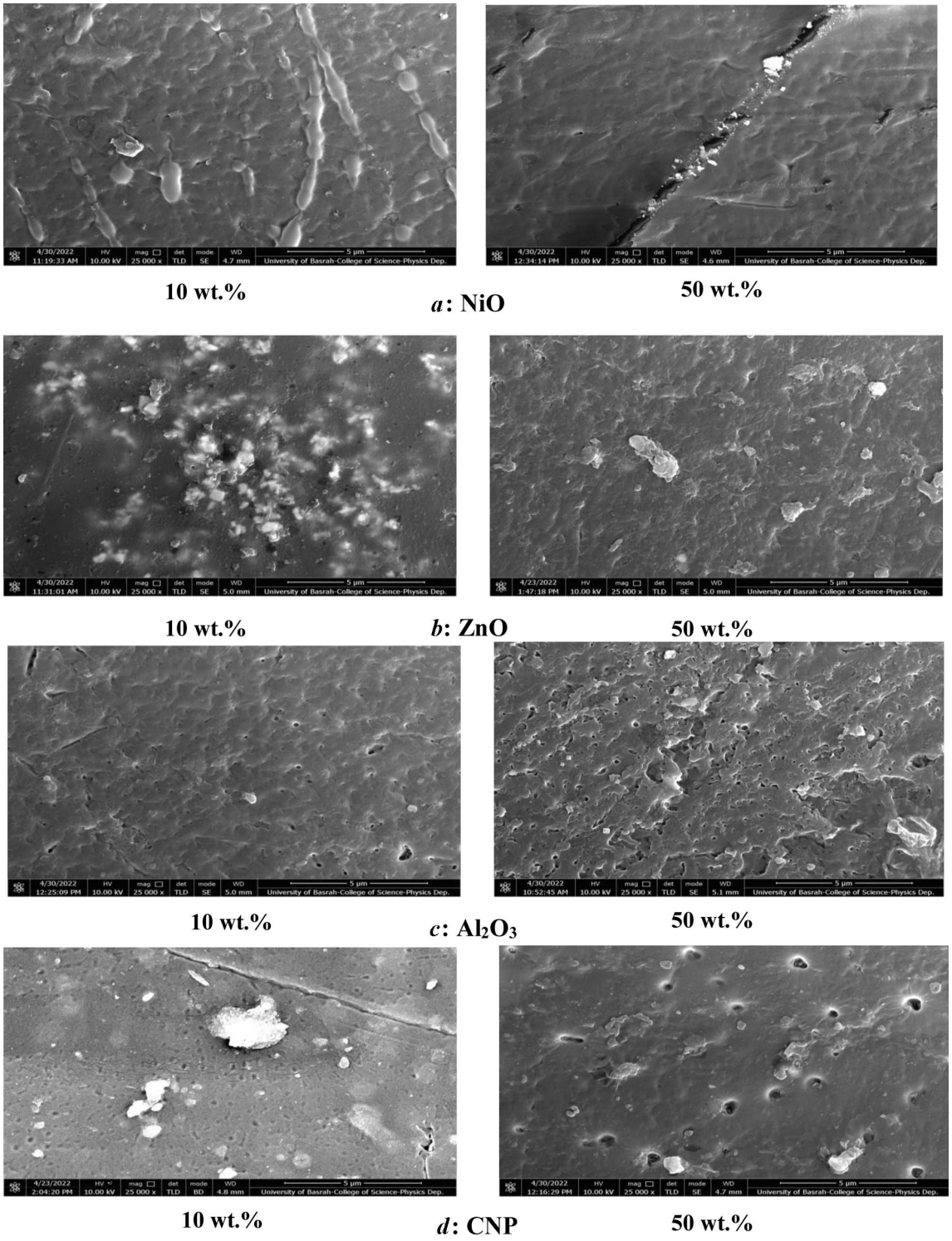

Fig. 5. Microstructure of the epoxy blend reinforced with (10–50 wt.%) of different powders

and (3). Fig. 6 illustrates the thermal conductivity of the epoxy blend composites as a function of the reinforcing materials' weight fractions.

Results indicate that the unreinforced epoxy blend (matrix) exhibits the lowest thermal conductivity, consistent with its properties as a good insulating material. All reinforced composites showed a similar trend: the thermal conductivity coefficient increased significantly and directly with the weight percentage of the reinforcing filler. Comparing the different composites, thermal conductivity varied considerably with filler type. The nickel powder (NiO)-reinforced composite achieved the highest thermal conductivity, surpassing all other composites including the unreinforced matrix. Zinc oxide (ZnO), aluminum oxide (Al_2O_3), and carbon nanoparticle (CNP) composites also demonstrated increased thermal conductivity relative to the base epoxy, though their enhancement percentages were lower than those of NiO. Comparative thermal conductivity values for all composites are presented in Table 2.

We observed that the carbon nanoparticle (CNP) composite exhibited the lowest thermal conductivity, which was reduced by 11.2–16.7% relative to the matrix across the 10–50 wt.% filler range. This reduction stems from the intrinsic thermal insulation properties of CNPs. Their presence disrupts heat transfer primarily through phonon-mediated conduction: atomic vibrations generate elastic waves (phonons) that propagate through both the matrix and CNPs. Due to mismatches in atomic structure and bonding between the epoxy matrix and CNPs, phonons encounter interfacial obstructions, scattering at these boundaries. This phonon scattering mechanism significantly suppresses thermal conductivity. Composites reinforced with Al_2O_3, ZnO, and NiO exhibited higher thermal conductivities, increasing by 19.5–31.3%, 28.0–38.7%, and 32.5–46.3% respectively across the same weight fraction range (10–50 wt.%). Despite the superior insulating performance of the CNP composite, all filled systems exceeded the thermal conductivity of the unreinforced epoxy matrix (0.938 $W/(m \cdot K)$). This demonstrates that incorporating any of these particulate fillers enhances the thermal conductivity of the epoxy blend [25]. Several factors govern the enhanced thermal conductivity of these composites relative to the matrix; (i) filler chemistry: metallic oxide reinforcements (Al_2O_3, ZnO, NiO) intrinsically exhibit high

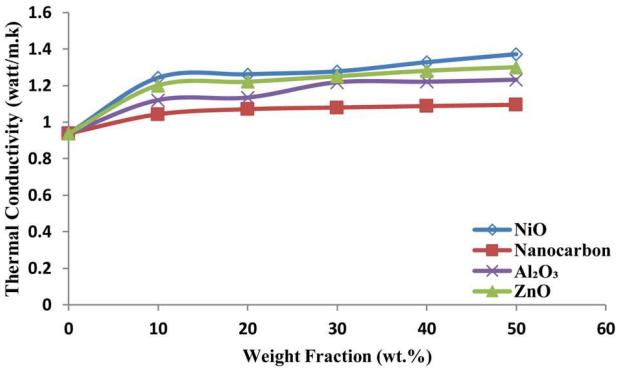

Fig. 6. Thermal conductivity of the epoxy blend resin reinforced with different powders

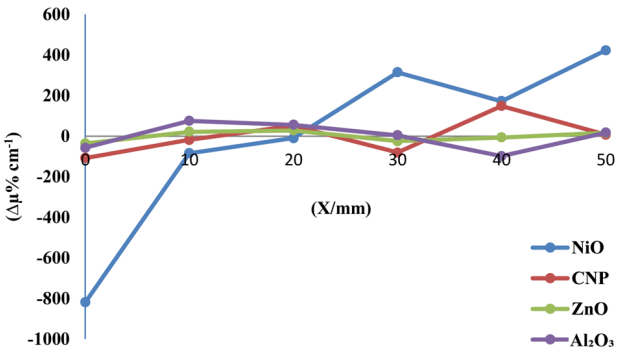

Fig. 7. Variation of the attenuation coefficient ($\Delta\mu\%$) by location in epoxy blends with different powders

Table 2. **Improvement in thermal conductivity with filler loading (10–50 wt.%)**

Composite type	Improvement percentage, %
Epoxy blend	0
NiO	32.5–46.3
ZnO	28–38.7
Al_2O_3	19.5–31.3
CNP	11.2–16.7

thermal conductivity. (ii) particle size and distribution: larger particles reduce phonon scattering by shortening thermal pathways. Though not directly observable via SEM imaging, these optimized paths exhibit greater stability due to minimized vibrational disturbances at interparticle contacts. (iii) filler loading: higher weight fractions increase particle density, further shortening thermal pathways [26]. Filler-matrix interface quality significantly influences composite thermal conductivity. Strong adhesion promotes effi-

Table 3. **Average values of the linear attenuation coefficient and standard deviation for the epoxy blend reinforced with various powders**

Type of reinforcement material	Average linear attenuation coefficient and standard deviation for the materials					
	0%	10%	20%	30%	40%	50%
NiO	0.205 ± 0.0817	0.041 ± 0.0083	0.0245 ± 0.0027	0.048 ± 0.0314	0.0162 ± 0.0172	0.072 ± 0.0421
Nanocarbon	0.205 ± 0.0475	0.117 ± 0.0082	0.049 ± 0.0222	0.178 ± 0.0355	0.048 ± 0.0655	0.091 ± 0.0033
ZnO	0.205 ± 0.0244	0.117 ± 0.0148	0.108 ± 0.0189	0.187 ± 0.0164	0.160 ± 0.0043	0.125 ± 0.0113
Al_2O_3	0.205 ± 0.0330	0.032 ± 0.0442	0.057 ± 0.0330	0.125 ± 0.0026	0.260 ± 0.0576	0.108 ± 0.0102

Table 4. **Comparison of the present research results with those reported in other studies**

Material (loading)	Study	Thermal conductivity W/(m · K	Improvement, % (vs. baseline)	Homogeneity	$\Gamma\mu$, cm^{-1} (energy)	Key findings
Unreinforced epoxy	Omar & Khadeer (current)	0.938	–	–	–	Higher baseline than typical epoxies
	(Park *et al.*, 2020) [30]	0.20–0.25	–	–	–	Standard epoxy baseline
NiO (50 wt.%)	Omar & Khadeer	1.37	46.3%	0.0421 (γ-ray attenuation)	0.072 [59.5 keV]	Micro-scale filler; voids at high loading reduce homogeneity/shielding
	(Al-Ghamdi *et al.*, 2016) [31]	0.75	275% (vs. 0.2)	Agglomeration at > 30 wt% [7]	–	Nano-NiO outperforms micro-NiO due to reduced phonon scattering
ZnO (50 wt%)	Omar & Khadeer	1.30	38.7%	0.0113 (γ-ray attenuation)	0.125 [59.5 keV]	Best homogeneity; superior low-energy gamma shielding
	(Rafiee *et al.*, 2010) [32]	1.40	600% (vs. 0.2)	SEM-based: 85% [6]	–	ZnO nanowires enable higher TC at low loadings
	(Naresh *et al.*, 2021) [33]	–	–	–	0.185 [0.662 MeV]	Bi_2O_3 composites match ZnO's shielding at higher energies

cient heat transfer, while weak interfaces (e.g., in NiO composites) restrict phonon transmission, reducing conductivity [27]. Furthermore, increasing filler loading (10–50 wt.%) elevates particle density within the composite. This shortens thermal conduction pathways, thereby enhancing overall thermal conductivity [28]. Crucially, filler distribution homogeneity determines conductivity outcomes; Uniform dispersion typically lowers thermal conductivity by maximizing phonon scattering. Aggregates and flakes from uneven distribution create localized percolation networks, increasing conductivity in NiO, ZnO, and Al_2O_3 composites [29].

3.2.2. Homogeneity test result

The proportions of powders and polymers within a polymeric blend composite significantly influence its durability and homogeneity. This test aims to assess the homogeneity of the prepared composites, with results presented in Fig. 7. As defined by Eq. (4), the material's homogeneity percentage can be determined by comparing the attenuation coefficient (μ) at specific measurement locations – derived from the transmitted intensity (I) – against the average attenuation coefficient (μ') across all locations. Fig. 7 illustrates the resulting homogeneity parameter ($\Delta\mu\%$) at five positions for the studied materials.

Figure 7 clearly shows the minimum $\Delta\mu\%$ values for the ZnO, CNP, and Al_2O_3 composites, respectively. In contrast, the NiO composite exhibits the highest $\Delta\mu\%$. These results indicate that the ZnO composite possesses superior homogeneity, while the NiO composite is the least homogeneous among the tested materials. Furthermore, homogeneity was assessed via the standard deviation of the linear attenuation coefficient. The ZnO composite demonstrated the lowest standard deviation (0.004–0.02%), significantly lower than those of the Al_2O_3, CNP, and NiO composites. This minimal deviation confirms the high homogeneity of the ZnO composite, signifying a uniform distribution of ZnO filler within the epoxy blend. Consequently, gamma ray energy is distributed and attenuated uniformly throughout the sample.

In contrast, other powdery composites exhibited significantly higher standard deviations. This indicates inferior homogeneity – ranging from semi-homogeneous to inhomogeneous – within these materials. Such non-uniformity concentrates gamma-ray energy in specific areas rather than distributing it evenly. Furthermore, defects like cavities and air bubbles, likely arising from localized agglomeration of reinforcement particles, contribute substantially to these elevated standard deviation values. The linear attenuation coefficient (μ) for γ-rays in the ZnO composite ranges from 0.108 cm^{-1} to 0.205 cm^{-1}. These values are significantly higher than those observed for the NiO composite (0.0162 cm^{-1} to 0.205 cm^{-1}), indicating ZnO's superior attenuation capability. Consequently, the ZnO composite demonstrates excellent gamma-ray shielding performance, while the NiO composite exhibits markedly lower effectiveness. This disparity stems from two primary factors; the lower density of NiO compared to ZnO, and the homogeneous distribution of ZnO particles within the epoxy matrix versus the heterogeneous distribution of NiO particles. This non-uniform dispersion in NiO directly compromises its radiation shielding efficacy, aligning consistently with the homogeneity results presented earlier (e.g., Fig. 7).

Discrepancies in NiO's thermal conductivity compared with the literature values (Table 4) arise from: (i) the use of micron-scale fillers in this study versus nano-NiO (50 nm) in [27], which reduces interfacial phonon scattering; (ii) the lower viscosity of the 50 : 50 epoxy blend enabling better particle integration than conventional resins. This highlights the sensitivity of composite performance to filler scale and matrix rheology.

4. Conclusions

This systematic investigation of carbon nanoparticles (CNP), Al_2O_3, NiO, and ZnO powders (10–50 wt%) within a 50 : 50 epoxy blend resin revealed distinct performance trade-offs governed by filler properties and dispersion. NiO composites achieved the highest thermal conductivity enhancement (46.3%, reaching 1.37 $W/(m \cdot K)$), leveraging its intrinsic high bulk thermal conductivity (92 $W/m \cdot K$); however, severe void formation and agglomeration at 50 wt.%, driven by the high density mismatch between NiO and the epoxy, trapped air during hand lay-up, and inherent irregular particle shape, created interfacial phonon scattering that capped further gains and critically impaired dispersion homogeneity (σ_μ up to 0.0421). Conversely, ZnO composites exhibited superior homogeneity (0.004–0.02%) due to their near-spherical particle shape and uniform distribution, which directly enabled exceptional gamma-ray shielding performance ($\mu = 0.205$ cm^{-1} for ^{241}Am at 59.5 keV) by maximizing photon interaction probability and leveraging Zn's high atomic number ($Z = 30$) for enhanced photoelectric absorption; this efficacy significantly outperformed NiO ($\mu = 0.072$ cm^{-1}), where heterogeneity created low-density gamma-ray pathways and reduced effective Z-density, and rivalled toxic alternatives like Bi_2O_3. While ZnO and Al_2O_3 showed more moderate thermal improvements (38.7% and 31.3% respectively), their defect-resistant morphology, particularly ZnO's ability to maintain structural integrity and even reduce cracks at 50 wt.% unlike others, provided balanced performance. CNP composites demonstrated limited thermal enhancement (11.2–16.7%) due to pronounced interfacial phonon scattering. Crucially, the morphology-loading interplay showed that all fillers integrated relatively well at 10 wt%, but at 50 wt%, NiO, Al_2O_3, and CNP developed significant voids/agglomerates, exposing viscosity limits of hand lay-up processing, whereas ZnO uniquely sustained compatibility. Consequently, ZnO emerges as the optimal filler for applications requiring harmonized thermal management, superior gamma-ray shielding, and structural homogene-

ity, while NiO's thermal advantages are offset by its dispersion limitations and poor shielding efficacy at higher loadings.

The authors extend their sincere gratitude to the Department of Physics, Faculty of Science, for providing the essential research facilities and academic support that were instrumental in completing this study. The department's scientific resources and expert guidance played a pivotal role in the success of this work.

1. B. Bilyeu, W. Brostow, K.P. Menard. Determination of volume changes during cure via void elimination and shrinkage of an epoxy prepreg using a quartz dilatometry cell. *Polimery* **46**, 799 (2001).
2. B. Bilyeu, W. Brostow, K.P. Menard. Epoxy thermosets and their applications. III. Kinetic equations and models. *J. Mater. Ed.* **23**, 189 (2001).
3. Z. Guo, X.T. Liang, R.S. Pereira, T. Hahn. CuO nanoparticle filled vinyl-ester resin nanocomposites: Fabrication, characterization and property analysis. *Compos. Sci. Technol.* **67** (10), 2036 (2007).
4. M. Singla, V. Chawla. Mechanical properties of epoxy resin-fly ash composite. *J. Miner. Mater. Charact. Eng.* **9** (3), 199 (2010).
5. H.M. Ali, R.A. Rasool, S.Y. Moustafa. Reinforcement effect of alumina and silica on the mechanical properties of mixture polyesters (Unsaturated Polyester/Polyurethane). *Rafidain J. Sci.* **29** (2), 36 (2020).
6. E.E. Khadeer, M.A. Abed, M.A. Hmood. The optical properties of unsaturated polyester reinforcement by glass fibers. *Jordan J. Phys.* **17** (2), 155 (2024).
7. J. Kim, P.H. Kang, Y.C. Nho. Positive temperature coefficient behavior of polymer composites having a high melting temperature. *J. Appl. Polym. Sci.* **92** (1), 394 (2004).
8. E.K. Hemadi, K.K. Al ahmady, E.Z. Sulyman. Improvement of mechanical and thermal properties of unsaturated polyester resin by adding iron residues. *College of Basic Educ. Res. J.* **20** (4), (2024).
9. S.L. Shindé, J.S. Goela. *High Thermal Conductivity Materials* (Springer, 2006) [ISBN: 0-387-25100-6].
10. B.M. Tyson, R.K.A. Al-Rub, A. Yazdanbakhsh, Z. Grasley. A quantitative method for analyzing the dispersion and agglomeration of nano-particles in composite materials. *Compos. Part B* **42**, 1395 (2011).
11. Thonon Hassaneh Hadi, Hussein Nour al-Din. Mechanical and physical properties of epoxy and unsaturated polyether complexes reinforced with glass fiber and nanomaterial alumina powder. *J. Educ. Sci.* **28** (1), 150 (2019).
12. M. Jahedi, M.H. Paydar, M. Knezevic. Enhanced microstructural homogeneity in metal-matrix composites developed under high-pressure-double-torsion. *Mater. Charact.* **104**, 92 (2015).
13. N.N. Greenwood, A. Earnshaw. *Chemistry of the Elements* (Elsevier, 2012) [ISBN: 0-7506-3365-4].
14. M. Nambo, K. Itami. *Synthesis of New Nanocarbon Materials* (Access Science, 2009).
15. T. Laird. *Ullmann's Encyclopedia of Industrial Chemistry* (VCH, 1996/1997).
16. A.O. Ameh, M.T. Isa, I. Sanusi. Effect of particle size and concentration on the mechanical properties of polyester/date palm seed particulate composites. Leonardo Electron. *J. Pract. Technol.* **14** (26), 65 (2015).
17. E.E. Ghadeer, R.Z.A. Al-Fulayih, Z.B. Ibraheem. Study of the effect of adding glass and carbon powders on optical behavior of unsaturated polyester resin. *AIP Conf. Proc.* **2394**, 090023 (2022).
18. E.E. Khadeer, T.M. Khudhur, R.Z.A. Al-Fulayih, Y. Al-Salman. Study of the effect of water and nitric acid on epoxy resin reinforced with different weight ratios of glass and carbon powder. *Oxid. Commun.* **48** (1), 4038 (2025).
19. J.E. Mark. (Ed.) *Physical properties of polymers handbook* (Springer, 2007) [ISBN-13: 978-0-387-69002-5].
20. M.J. Ahmed. *To Fabricated and Study Mechanical Properties and Homogeneous of (Al–Zn–Mg) Alloy Matrix Composite*. M.Sc. Thesis, College of Education, University of Mosul, Iraq (2013).
21. M.T. Tcil, C.S. Mahajan, R. Nathuram. Measurement of mass and Linear attention coefficient of gamma rays for various through aqueous soloution of salts. *Indian J. Pure* **39**, (2001).
22. V.D. Cherkasov, V.V. Avdonin, Y.V. Yurkin, Y.P. Scherbak, M.E. Buzoverya, I.A. Karpov, V.O. Pilshchikov. Research of radiation resistance of polymer composite materials. *Mater. Phys. Mech.* **44** (3), 433 (2020).
23. K.W.Y. Al-Baroudi. *Effect of Changing the Weight Fractions of Different Powders on Some Physical Properties of Epoxy Composites*. M.Sc. Thesis, University of Mosul, College of Science, Mosul, Iraq (2021).
24. C.A. Chatham, T.E. Long, C.B. Williams. A review of the process physics and material screening methods for polymer powder bed fusion additive manufacturing. *Prog. Polym. Sci.* **93**, 68 (2019).
25. R. Kochetov, T. Andritschet, U. Lafont, H.F. Morshuis Peter. Thermal conductivity of nano-filled epoxy systems. *Proc. IEEE Conf. Electr. Insul. Dielectr. Phenom.* 538 (2009).
26. R. Atif, I. Shyha, F. Inam. Mechanical, thermal, and electrical properties of graphene-epoxy nanocomposites–A review. *Polymers* **8** (8), 281 (2016).
27. J. Hu, X. Ruan, Y.P. Chen. Thermal conductivity and thermal rectification in graphene nanoribbons: A molecular dynamics study. *Nano Lett.* **9** (7), 2730 (2009).
28. J. Che, T. Cagin, W.A. Goddard III. Thermal conductivity of carbon nanotubes. *Nanotechnology* **11** (2), 65 (2000).
29. D.Y. Jiang, Q. Zhang, G. Chen, S.F.Yoon, J. Ahn, S.G. Wang, Q. Zhou, Q. Wang, J.Q. Li. Thermal conductivity of multiwalled carbon nanotubes. *Phys. Rev. B* **66** (16), 165440 (2002).

30. S. Park, Y. Lee, B. Kim, J.H. Kim, Y.G. Jeong. Thermal conductivity and mechanical properties of epoxy composites filled with aluminum nitride and boron nitride nanotubes. *Composites Part B: Engineering* **202**, 108428 (2020).
31. A.A. Al-Ghamdi, H.A. Al-Turaif, A.A. Abdelaziz. Epoxy/nickel oxide nanocomposites: Fabrication, evaluation of physical properties. *J. Mater. Sci.* **51**, (22), 10146 (2016).
32. M.A. Rafiee, J. Rafiee,I. Srivastava, Z. Wang, H. Song, Z.-Z. Yu., N. Koratkar. Enhanced mechanical properties of nanocomposites at low graphene content. *ACS Nano* **4** (12), 7415 (2010).
33. K. Naresh, K. Shukla, V. Choudhary, B.S. Tomar. Role of Bi_2O_3 on shielding of epoxy composites against gamma radiation. *Radiation Phys. Chem.* **179**, 109267 (2021).

Received 18.06.24

С.К. Омар, Е.Е. Хадір

ВИВЧЕННЯ ВПЛИВУ МАСОВОЇ ЧАСТКИ ПОРОШКІВ РІЗНИХ ТИПІВ НА ТЕПЛОПРОВІДНІСТЬ ТА ГОМОГЕННІСТЬ СУМІШІ ЕПОКСИДНОЇ СМОЛИ

У цьому дослідженні вивчався вплив масових часток (10–50 мас.%) вуглецевих наночастинок (CNP), а також порошків Al_2O_3, NiO та ZnO на теплопровідність та гомогенність епоксидної суміші у співвідношенні 50 : 50. Сканувальна електронна мікроскопія (SEM) виявила різні морфології поверхні: композити NiO мали гладенькі поверхні з мінімальними проміжками за низьких концентрацій, але утворювали великі порожнечі при 50 мас.%, тоді як поверхні Al_2O_3 демонстрували тріщини та посилене утворення бульбашок у разі вищих рівнів наповнення. Композити ZnO та CNP мали шорсткі, пористі поверхні зі значною агломерацією при 50 мас.%. Всі наповнювачі покращили теплопровідність суміші порівняно з чистою епоксидною смолою (0,938 Вт/(м · K)), причому найбільше покращення продемонстрував NiO (32,5–46,3%), далі йдуть ZnO (28–38,7%), Al_2O_3 (19,5–31,3%) та CNP (11,2–16,7%). Тести для визначення рівня гомогенності за допомогою методу ослаблення гамма-випромінювання (джерело ^{241}Am) показали, що композити ZnO досягли найвищої однорідності (найнижчий $\Delta\mu$% та стандартне відхилення $\sigma_\mu = 0,004$–0,02%), тоді як композити NiO були найменш однорідними. Важливо, що рівномірний розподіл частинок ZnO також забезпечив краще екранування гамма-випромінювання ($\mu = 0,108$–0,205 см$^{-1}$), тоді як гетерогенність NiO погіршувала ефективність його ослаблення.

Ключові слова: оксид алюмінію (Al_2O_3), вуглецеві наночастинки (CNP), епоксидна суміш, ослаблення гамма-випромінювання, тест на гомогенність, оксид нікелю (NiO), полімерний композит, сканувальна електронна мікроскопія (SEM), теплопровідність, оксид цинку (ZnO).